Angewandte Chemie
Eine Zeitschrift der Gesellschaft Deutscher Chemiker

Supporting Information

Highly Efficient Spatially–Temporally Synchronized Construction of Robust Li_3PO_4-rich Solid–Electrolyte Interphases in Aqueous Li-ion Batteries

*X. Zhu, Z. Lin, J. Lai, T. Lv, T. Lin, H. Pan, J. Feng, Q. Wang, S. Han, R. Chen, L. Chen, L. Suo**

Methods

Materials Characterizations

The crystal structure of Li_3PO_4 powder was identified on a Bruker D8 Phaser X-ray diffractometer with Cu-Kα radiation ($\lambda = 1.5406$ Å). Field emission scanning electron microscopy (FESEM, Hitachi S-4800, Japan) and atomic force microscopy (AFM, Agilent 550, Agilent Technologies) were employed to analyze the surface topography of the titanium foil electrodes. X-ray photoelectron spectroscopy (XPS, Thermo Scientific ESCALab 250Xi) and Time of Flight Secondary Ion Mass Spectrometry (TOF-SIMS, IONTOF TOF.SIMS 5) were carried out to identify the composition of the SEI layer. High-resolution transmission electron microscopy (HRTEM, FEI Titan Cubed Themis G2 300) was used to investigate the interplanar spacing of the SEI layer. Before HRTEM testing, the TiO_2 and TiO_2@5%LHPO electrodes were soaked in deionized water and washed three times with de-ionized water to eliminate any residual lithium salts. The melting point of 10m LiTFSI was determined using a differential scanning calorimeter (DSC, NETZSCH, DSC 214). The viscosity variations of 10m LiTFSI electrolyte at different temperatures were measured using a Brookfield rheometer (DV next).

Electrode preparation and electrochemical measurement.

Bistrifluoromethanesulfonimide lithium salt (LiTFSI, 98%) was purchased from Shandong Hairong Corporation. The graphite and $LiMn_2O_4$ powder were purchased from MTI Corporation. The TiO_2 (Anatase, 25 nm, 98%) powder and de-ionized (DI) water (HPLC grade) were purchased from Sigma-Aldrich. The lithium dihydrogen phosphate (LiH_2PO_4, 97%) was bought from Alfa Aesar. The Ti eletrodes were cut to 1 × 1 cm. The graphite or graphite@5%LHPO electrode was prepared by

compressing active material (graphite or graphite@5%LHPO, Super P®, and polytetrafluoroethylene (PTFE) at a weight ratio of 8:1:1 onto the aluminum mesh (1 × 1 cm). The working electrode was made by combining active materials ($LiMn_2O_4$, TiO_2@x%LiH_2PO_4 (x = 0, 2, 5, and 10), TiO_2@5%$KHCO_3$ and $Li_4Ti_5O_{12}$), Super P®, and polyvinylidene fluoride (PVDF) in an 80:10:10 weight ratio using 1-Methyl-2-pyrrolidinone (NMP) as the solvent. The obtained slurry was coated on aluminum foil and vacuum-dried for 6 hours at 120 °C to form the working electrodes. The loading mass of $LiMn_2O_4$ cathode, TiO_2@x% LHPO electrode was ~6, ~3, and ~3 mg cm^{-1}, respectively. The amount of electrolyte added to the mini pouch cell is 50 μL.

The linear sweep voltammetry (LSV) curves were recorded on a CHI660E electrochemical workstation with a three-electrode system, using Ti poil, graphite or graphite@5%LHPO electrode as the working electrode, Pt net as the counter electrode, and Ag/AgCl as the reference electrode with scanning rates of 10 mV s^{-1}. Mini pouch-type cells were assembled to evaluate the electrochemical performance of the $LiMn_2O_4$//TiO_2 and $LiMn_2O_4$//TiO_2@5%LHPO full cells. The assembled mini pouch-type cells were galvanostatically tested between 0.8−2.5 V using a multichannel battery test system (Land CT3001A). The in situ differential electrochemical mass spectrometry (DEMS) test was conducted using a commercial mass spectrometer (Hiden, Beijing) coupled with assembled Swagelok cells containing $LiMn_2O_4$ positive electrode, TiO_2, or TiO_2@5%LHPO anode, glass fiber separator, and 150 μL electrolytes. Before testing, the airtight Swagelok cells were ventilated for two hours with ultrahigh-purity Ar (99.999%) to eliminate impurity gas. The continuous pure Ar gas (0.5 mL min^{-1}) was then permitted to *in situ* monitor the gas released from the inner space of the cell, which was then analyzed by the mass spectrometer. Electrochemical impedance spectroscopy (EIS) measurements on these full cells were carried

out using a Zahner (IM6e, Germany) electrochemical workstation. The alternating voltage amplitude in the impedance measurements was 10 mV, and the frequency ranged from 100 mHz to 4 MHz. The Nyquist plots from the EIS measurements were fitted with the most appropriate circuit model using the Zview software. The viscosity of the 10 m LiTFSI electrolyte was evaluated using a Brookfield viscometer (DV2T LV) with a controlled shear rate and shear stress at 25 ℃. The Zahner electrochemical workstation was employed to measure the ionic conductivity of 10 m LiTFSI electrolyte at a set temperature by using the a.c. impedance method. Differential scanning calorimetry was conducted by using a DSC1 (Mettler-Toledo) from −70 °C to 50 °C at a heating rate of 2 °C min^{-1}, with the sample maintained at −70 °C for 5 minutes before testing.

Chemical verification of the formation of Li_3PO_4 in 1m LiTFSI aqueous solution.

Firstly, 2.87 g LiTFSI was dissolved in 10 g deionized water to prepare 1m LiTFSI aqueous solution, then added 0.5g LiH_2PO_4 was added and thoroughly dissolved by vigorous shaking. Finally, 0.5g of LiOH was added to the solution, and after thorough mixing, a white precipitate was produced.

Evaluation of the effectiveness of adding LiH_2PO_4 to the anode instead of the electrolyte.

Due to the influence of the "common ion effect", the dissolution of LiH_2PO_4 will be inhibited in a high concentration electrolyte, so we added LiH_2PO_4 to the electrode to keep the dissolution equilibrium only at the anode interface. By doing this, it is sufficient to keep the ionization balance of $H_2PO_4^-$ at the negative electrode interface even in a high concentration electrolyte. Thus, the passivation behavior of inactive graphite electrodes without (graphite) and with additional LiH_2PO_4 (graphite@P) in 10m LiTFSI electrolyte utilizing Pt electrode as

the counter electrode was studied using cyclic voltammetry (CV), and the results are presented in **Figure S7**. The graphite@P electrode exhibits a high hydrogen evolution potential during the first scan than the bare graphite electrode but a lower hydrogen evolution potential during the second scan. The HER of graphite@P happens early in the first cycle due to the fact that $H_2PO_4^-$ ionizes a portion of H^+ upon dissolution in the electrolyte, making the negative electrode interface weakly acidic. After the first cycle of scanning, the OH^- generated by the HER (**equation 2, Figure S1**) combines with H^+ (**equation 6**) to cause the ionization balance of $H_2PO_4^-$ to shift to the right (from **equation 3** to **5**), eventually forming insoluble Li_3PO_4 coated on the surface of the graphite electrode (**equation 7**). This passivation layer successfully prevents the HER from progressing further.

Calculation of the amount of charge consumed by the parasitic reaction and HER.

1 mAh/g = $1\times10^{-6}\times3600$ A·s/mg = 0.0036 C/mg

$F = e\cdot N_A$ = 96485 C/mol

(1) The amount of charge consumed by the parasitic reaction：

Q_1 = (Charge specific capacity − Discharge specific capacity) × 0.0036 (C/mg)

(2) The amount of charge consumed by the HER：

Q_2 = (Molar quantity electrons consumed by HER) × F

= (Molar quantity of H_2) × 2 × F (C/mg)

- $2H^+ + 2e^- \rightarrow H_2\uparrow$ (1)

or

- $2H_2O + 2e^- \rightarrow H_2\uparrow + 2OH^-$ (2)

- $H_3PO_4 \leftrightarrow H_2PO_4^- + H^+$ (3)
- $H_2PO_4^- \leftrightarrow HPO_4^{2-} + H^+$ (4)
- $HPO_4^{2-} \leftrightarrow PO_4^{3-} + H^+$ (5)
- $H^+ + OH^- \rightarrow H_2O$ (6)
- $3Li^+ + PO_4^{3-} \rightarrow Li_3PO_4\downarrow$ (7)

Figure S1 Digital photo of white powder produced by chemical verification process.

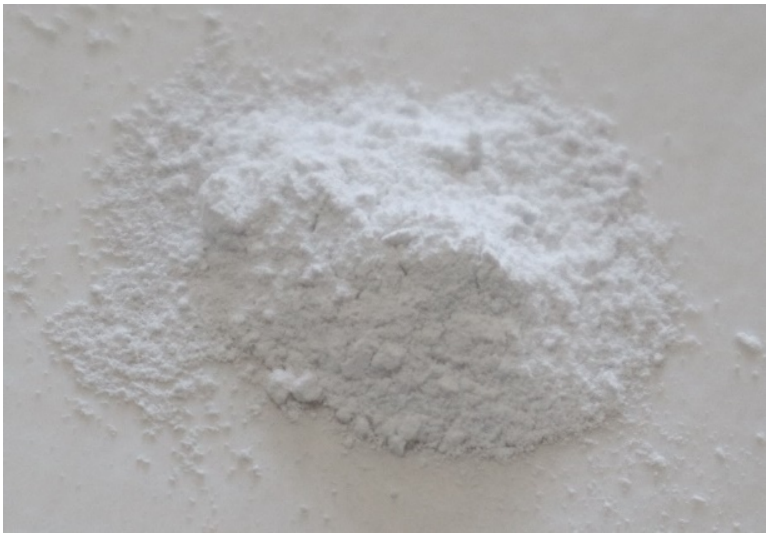

Figure S2 Digital photo of white powder produced by chemical verification process.

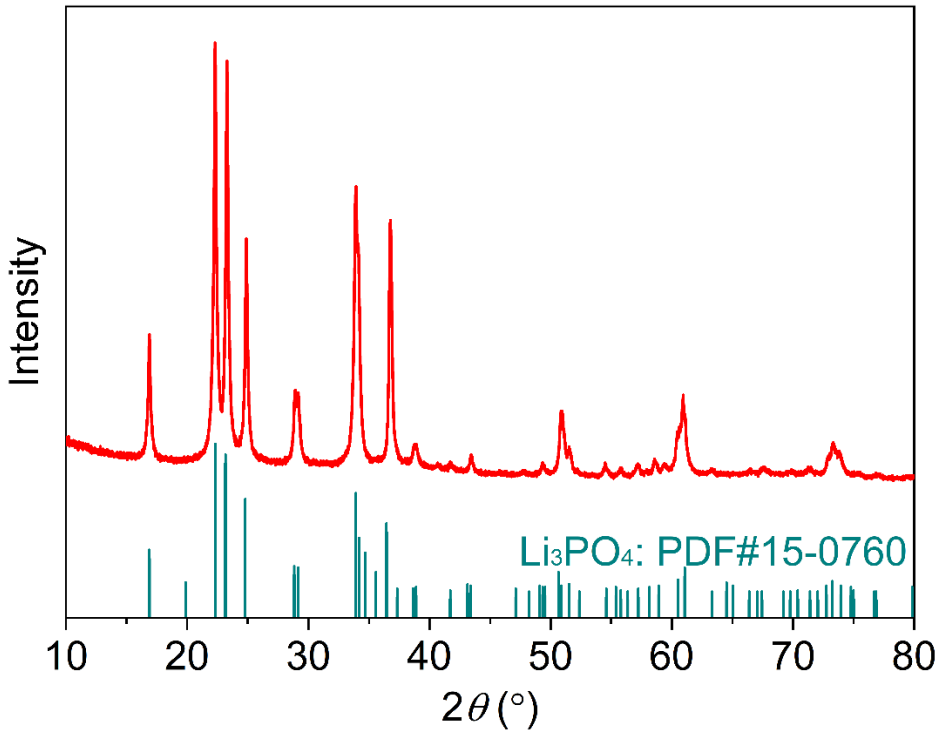

Figure S3 XRD pattern of the white precipitate.

Figure S4 SEM image of bare Ti foil.

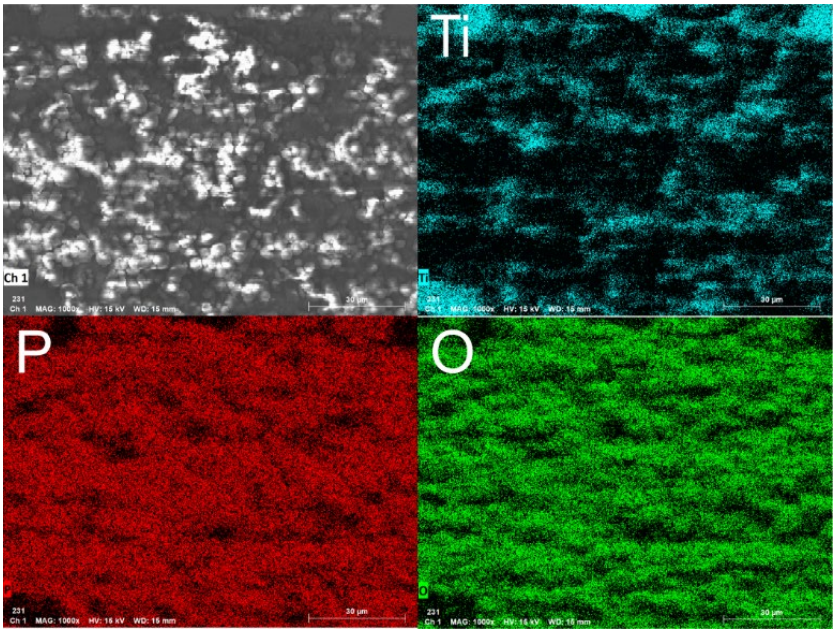

Figure S5 Elemental mapping images of the Ti foil after twice LSV scanning from 0 to −2.5 V in the 1m LiTFSI + 0.1m LiH_2PO_4 aqueous electrolytes.

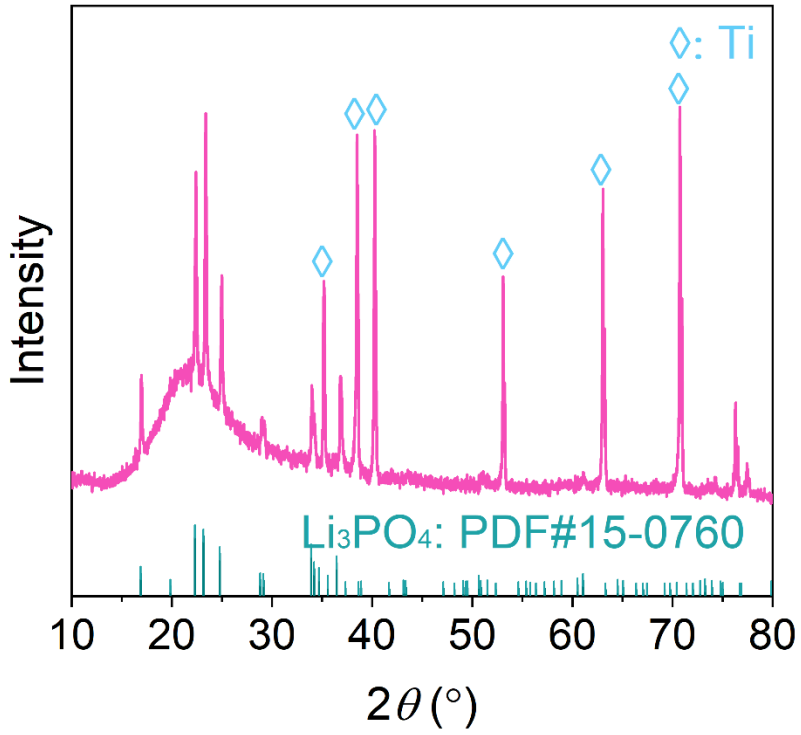

Figure S6 XRD pattern of the white precipitate on the Ti foil after twice LSV scanning from 0 to −2.5 V in the 1 m LiTFSI + 0.1 m LiH_2PO_4 aqueous electrolytes.

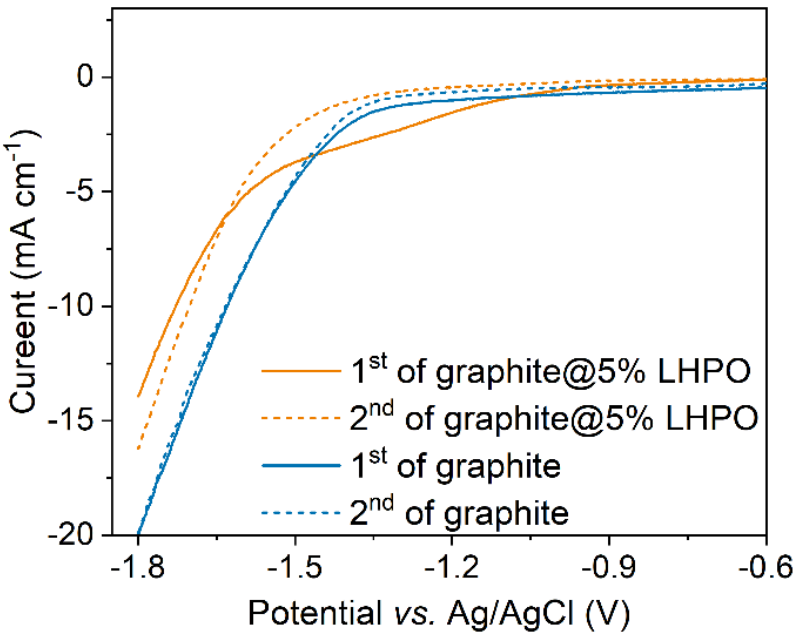

Figure S7 LSV curves of graphite@5%LHPO and graphite electrode in 10 m LiTFSI aqueous electrolyte.

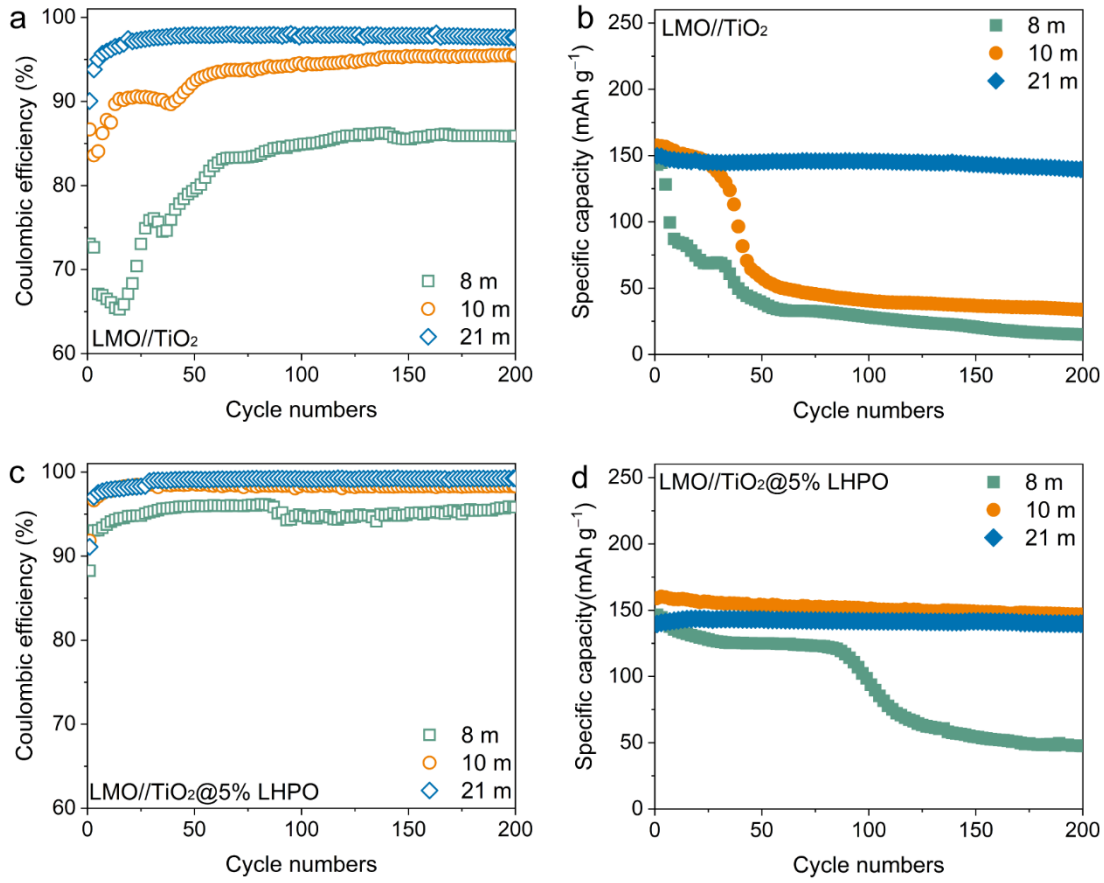

Figure S8 The Coulombic efficiencies, and cycling performances during 200 cycles at 0.5C of the LMO//TiO_2 (x = 0, 5) full cells in different concentration aqueous electrolytes.

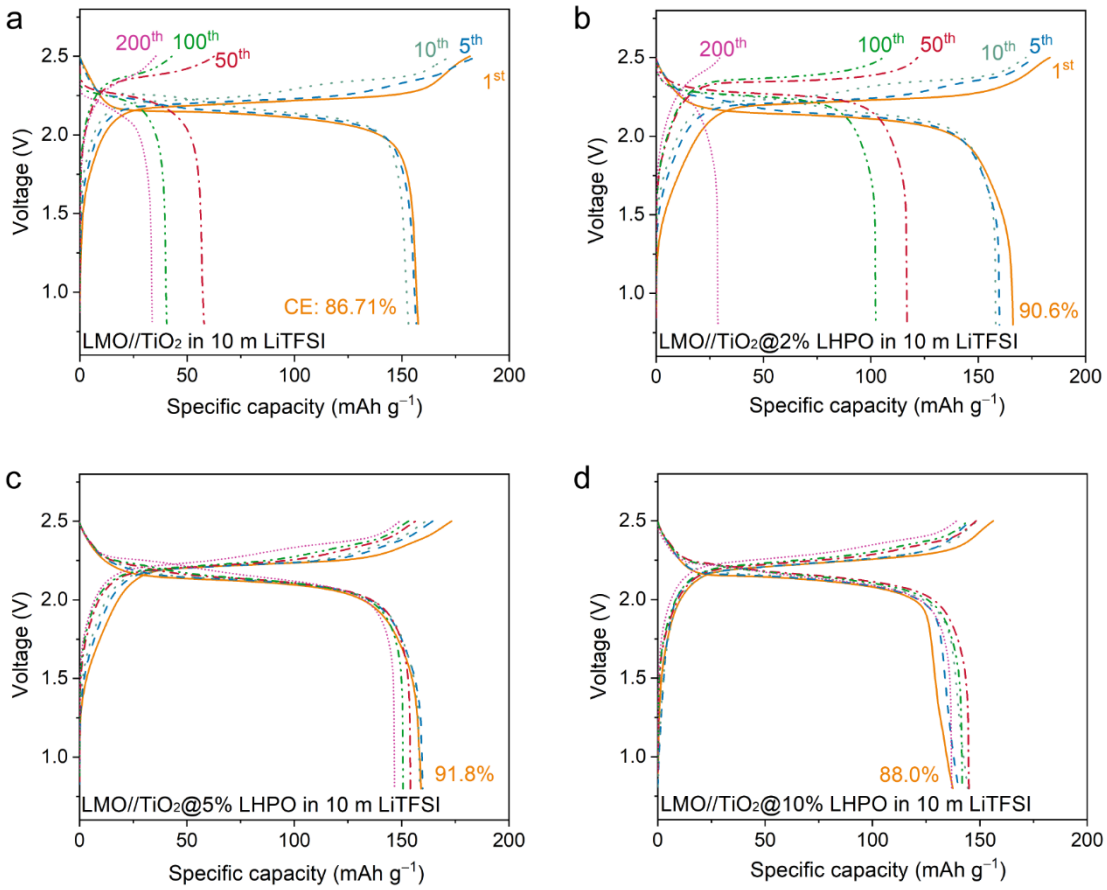

Figure S9 The charge-discharge curvers during 200 cycles at 0.5C of the LMO//TiO_2 (x = 0, 2, 5, and 10) full cells in 10 m LiTFSI aqueous electrolyte.

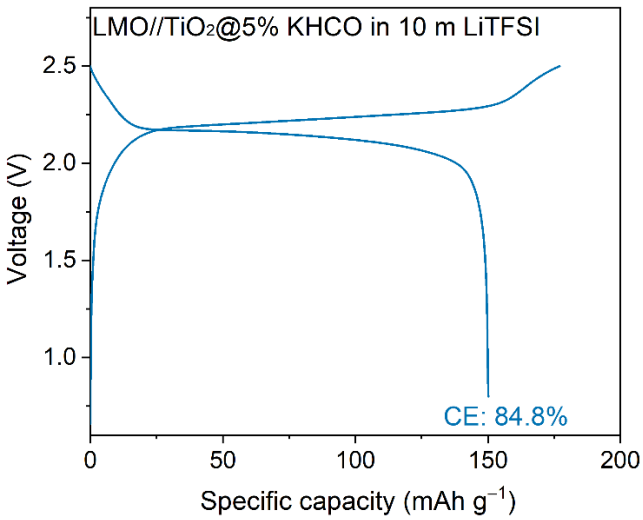

Figure S10 The charge-discharge curve of the LMO//TiO_2@5%$KHCO_3$ full cell at 0.5C in 10 m LiTFSI aqueous electrolyte.

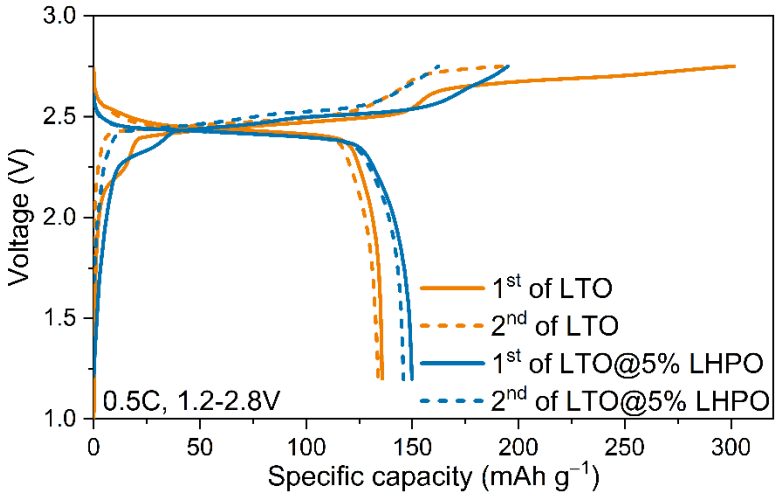

Figure S11 The initial two charge-discharge curves of the LMO//LTO and LMO//LTO@5%LHPO full cells at 0.5C in 28 m WiBS aqueous electrolyte.

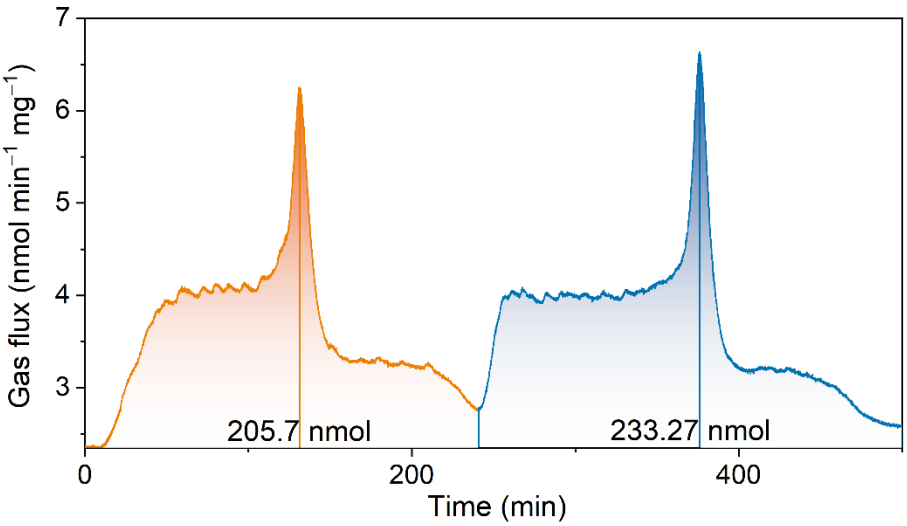

Figure S12 The total H_2 gas accumulation of the LMO//TiO_2 full cell during the two cycles.

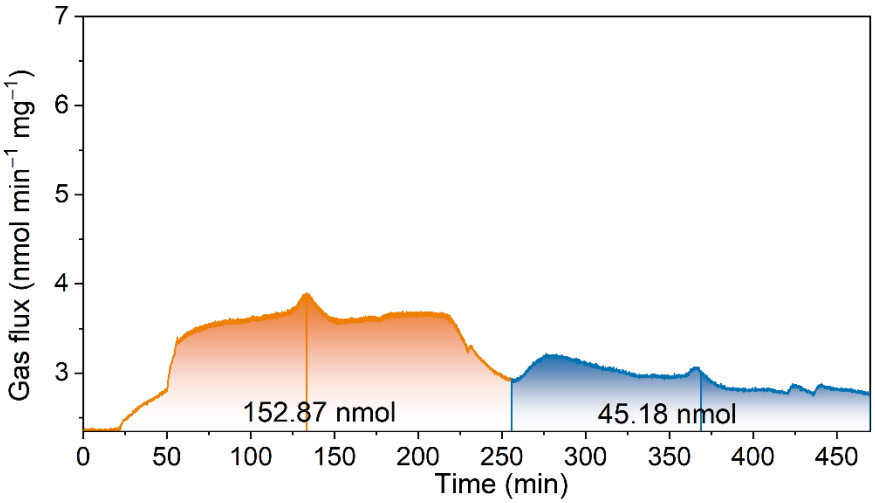

Figure S13 The total H_2 gas accumulation of the LMO//TiO_2@5%LHPO full cell during the two cycles.

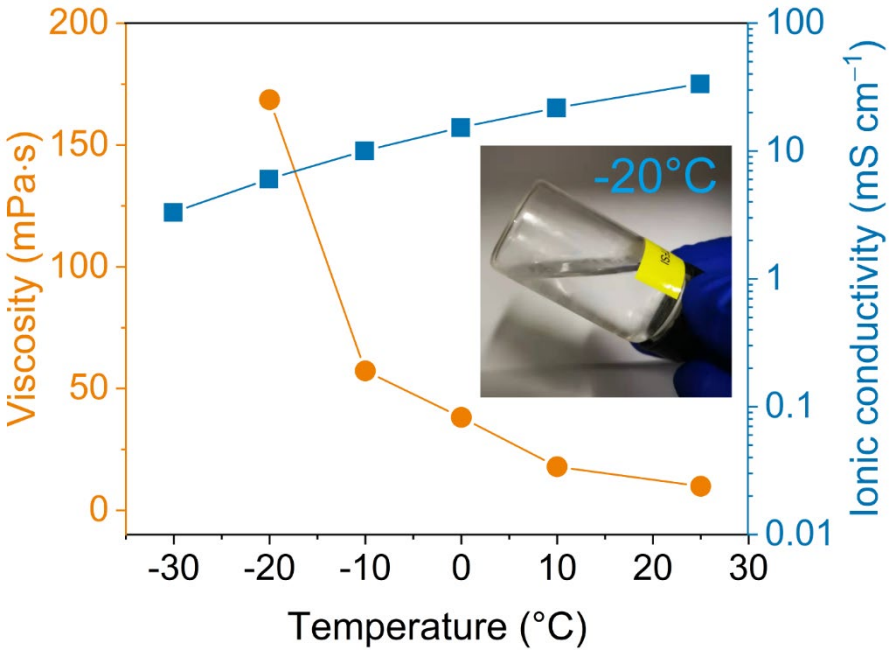

Figure S14 The temperature-dependent viscosities and ionic conductivities of the 10 m LiTFSI solution.

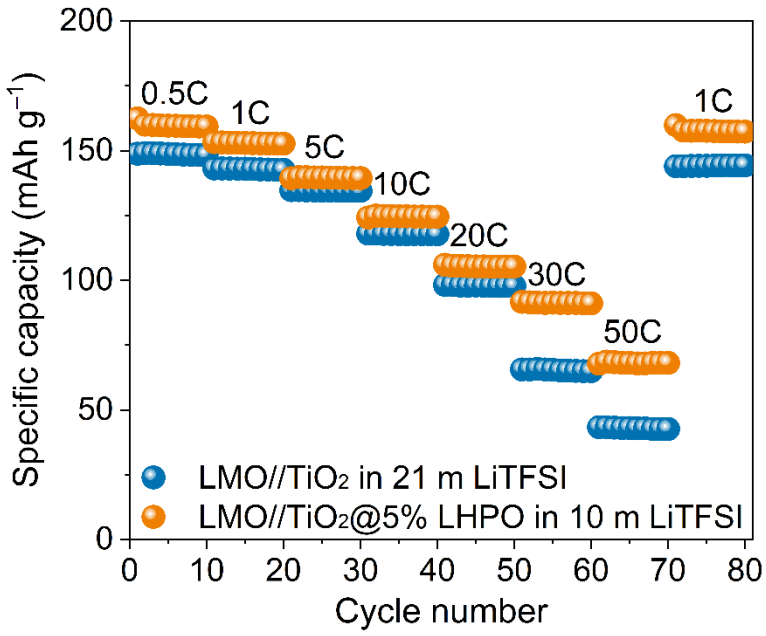

Figure S15 Rate performences of the LMO||10 m LiTFSI||TiO_2@5%LHPO and LMO||21 m LiTFSI||TiO_2 full cells.

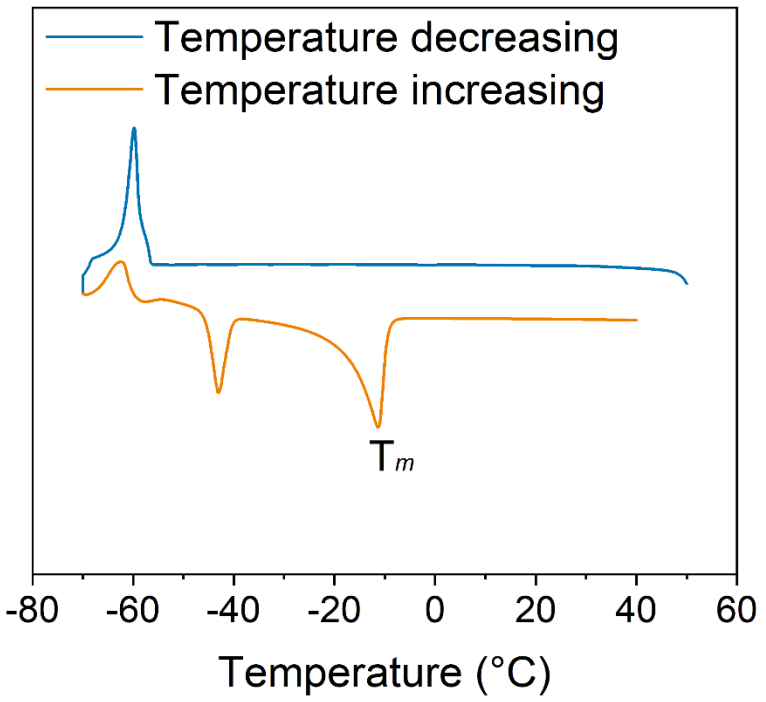

Figure S16 DSC measurement of 10m LiTFSI in H_2O.

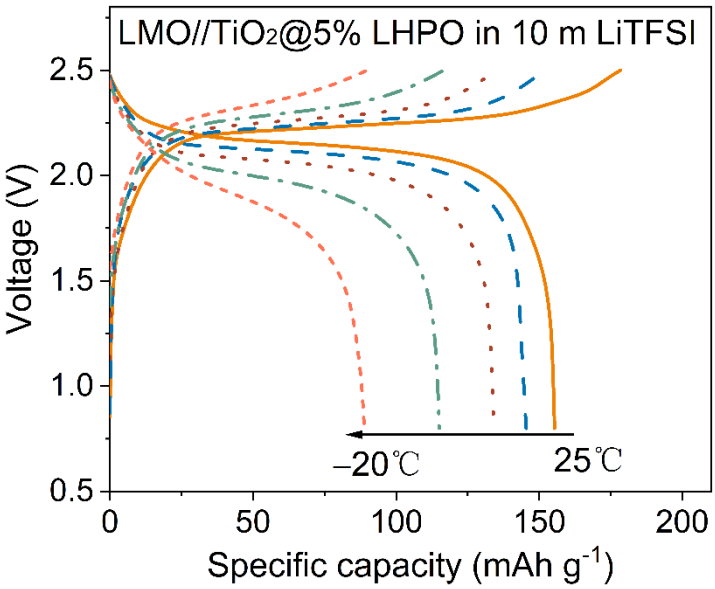

Figure S17 Charge-discharge profiles of the LMO//TiO_2@5% LHPO full cell at various test temperatures.

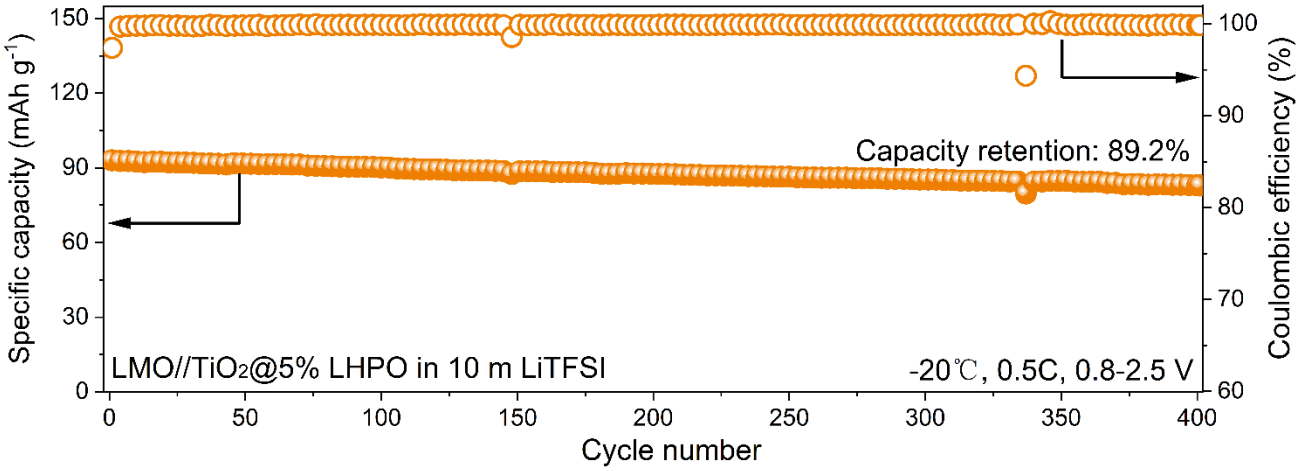

Figure S18 Cycling performance of the LMO//TiO_2@5% LHPO full cell under the low temperature of −20 ℃ at 0.5C.

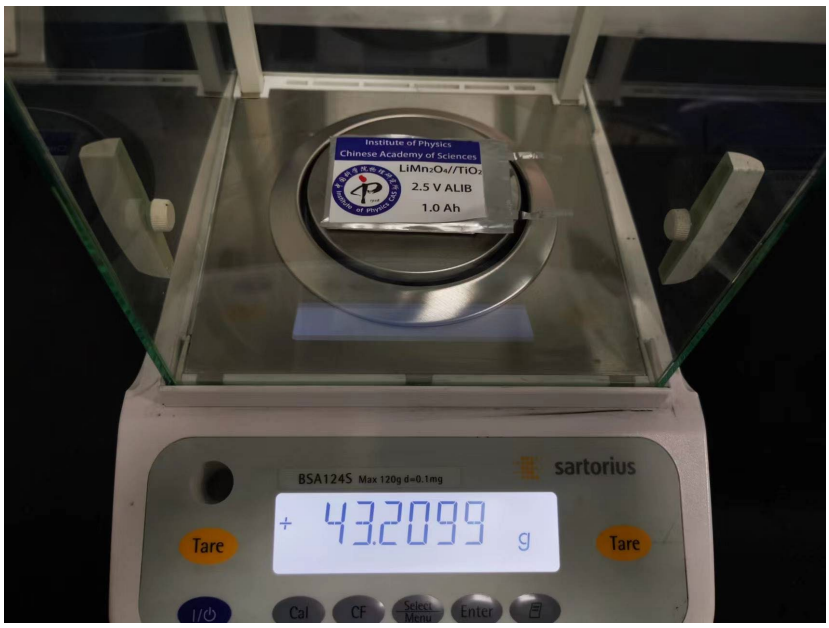

Figure S19 The weight of the Ah-level LMO//TiO_2@5%LHPO pouch cell.

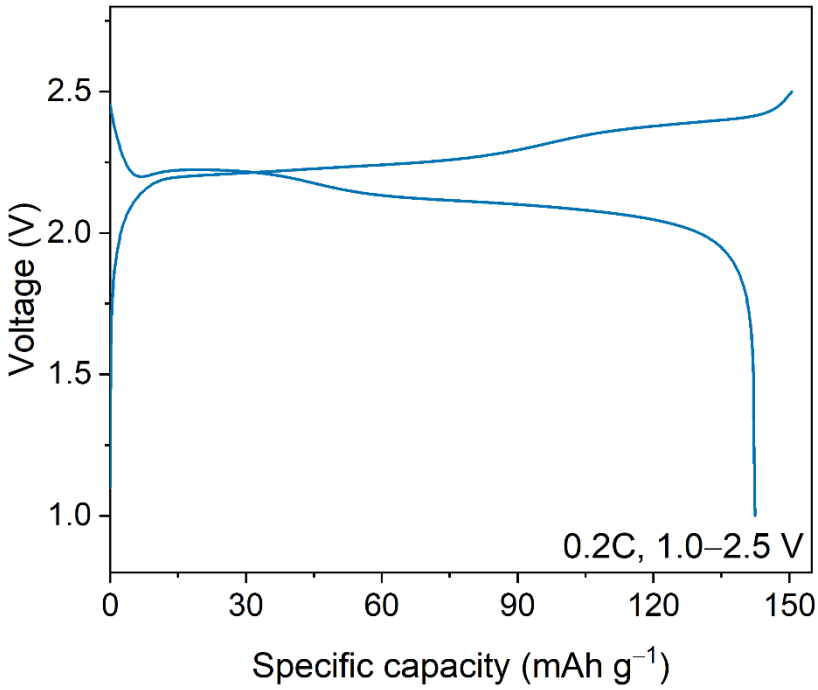

Figure S20 The initial charge-discharge profile of the Ah-level LMO//TiO_2@5%LHPO pouch cell at 0.2C in 10 m LiTFSI electrolyte.

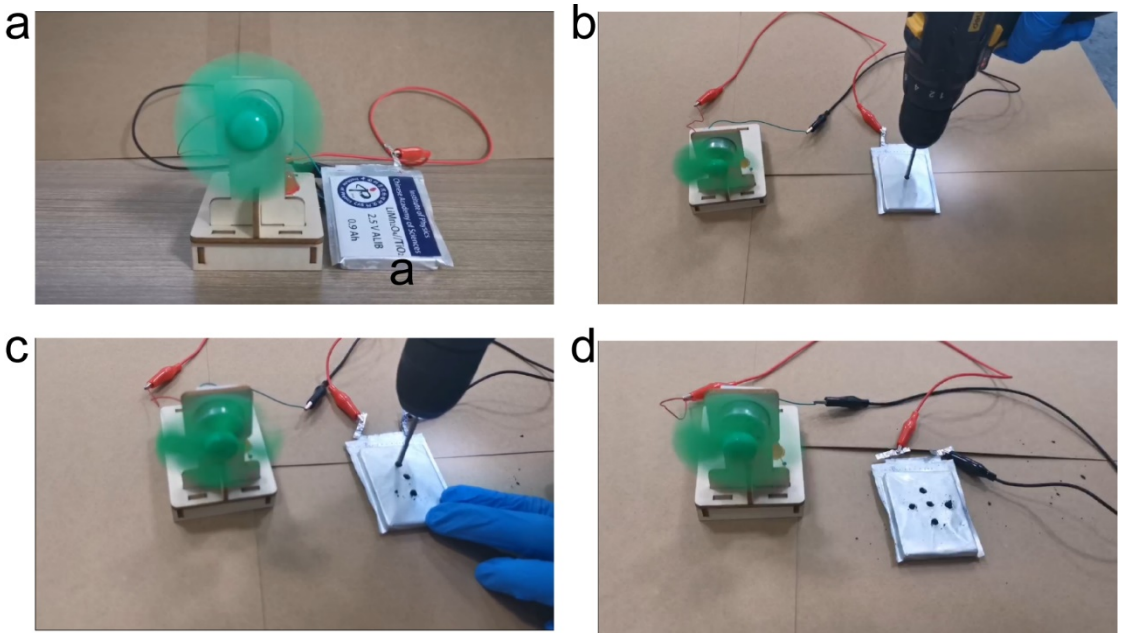

Figure S21 Drilling experiment of the Ah-level LMO//TiO_2 pouch cell.

Table S1 The solubility of inorganic Li salts in the water (g/100 g H_2O, 25 ℃, 1 atm).

inorganic salt	Solubility (g/100g H_2O, 25 ℃)
Li_2O	6.67
LiOH	12.80
Li_2CO_3	1.33
LiF	0.16
Li_3PO_4	0.039

Table S2 The average Coulombic efficiency (ACE, %) during 200 cycles at 0.5C of the LMO//TiO_2@*x*% LHPO (*x* = 0, 2, 5, 10) full cells in different concentration (8 m, 10 m, 21 m) aqueous electrolyte.

LHPO (%) / Electrolyte (m)	0	2	5	10
8	81.84	--	95.08	--
10	93.39	95.68	98.30	97.90
21	97.57	--	98.96	--

Table S3 The capacity fading per cycle (CFP, %) after 200 cycles at 0.5C of the LMO//TiO_2@*x*% LHPO (*x* = 0, 2, 5, 10) full cells in different concentration (8 m, 10 m, 21 m) aqueous electrolyte.

LHPO (%) / Electrolyte (m)	0	2	5	10
8	0.45	--	0.34	--
10	0.39	0.41	0.04	0.04
21	0.03	--	0.01	--

Table 4 Comparison of different high-voltage ALIBs systems.

Electrochemical couple	Average discharge voltage (V)	Electrolyte	Lithium Salt (*wt*%)	Cosolvent or additive (*wt*%)	H_2O (*wt*%)	Li:H_2O	Ionic conductivity (mS cm^{-1})	Ref.
$LiMn_2O_4/TiO_2$	2.1	10 m LiTFSI in H_2O	LiTFSI: 74.2	--	25.8	1:5.6	33.4 (25 ℃)	This work
$LiMn_2O_4/Mo_6S_8$	1.8	"Water-in-Salt" 21 m LiTFSI	LiTFSI: 85.8	--	14.2	1:2.6	8.3 (25 ℃)	[1]
$LiMn_2O_4/TiO_2$	2.1	13.8m LiTFSI + 1m TEAOTf	LiTFSI: 75.6	TEAOTf: 5.3	19.1	1:4	22 (25 ℃)	[2]
$LiMn_2O_4/TiO_2$	2.1	"Water-in-Bisalt" 21m LiTFSI+7m LiOTF	LiTFSI: 74.2 LiOTF: 13.6	--	12.2	1:2.0	6.5 (25 ℃)	[3]
$LiMn_2O_4/TiO_2$	2.1	21m LiTFSI+1.05m PAM	LiTFSI: <85.8	PAM: --	<14.2	1:2.6	--	[4]
$LiCoO_2/Li_4Ti_5O_{12}$	2.35	"Hydrate melt electrolyte" $Li(TFSI)_{0.7}(BETI)_{0.3}\cdot 2H_2O$ 19.4m LiTFSI+8.3m LiBETI	LiTFSI: 56.9 LiBETI: 32.8	--	10.3	1:2.0	3.0 (30 ℃)	[5]
$LiCoO_2/Li_4Ti_5O_{12}$	2.35	"Monohydrate Melt" $Li(PTFSI)_{0.6}(TFSI)_{0.4}\cdot H_2O$ 22.2m LiTFSI-33.3m LiPTFSI	LiTFSI: 34.2 LiPTFSI: 60.4	--	5.4	1:1	0.1 (30 ℃)	[6]
$LiMn_2O_4/Li_4Ti_5O_{12}$	2.45	63m "Water-in-Hybrid-Salt" 42m LiTFSI + 21m $Me_3EtN\cdot TFSI$	LiTFSI: 58.0	$Me_3EtN\cdot TFSI$: 37.2	4.81	1:1.3	0.91 (25 ℃)	[7]
$LiNi_{0.5}Mn_{1.5}O_4/Li_4Ti_5O_{12}$	3.0	"Hybrid Aqueous/Nonaqueous" 21m LiTFSI in H_2O+9.25m LiTFSI in DMC (H_2O/ DMC = 1:1, mass ratio)	LiTFSI: 79.2	DMC: 13.7	7.1	1:1.43	5.0 (30 ℃)	[8]
$LiMn_2O_4/Li_4Ti_5O_{12}$	2.40	"Molecular crowding" electrolyte 33.33m LiTFSI + 39.17m PEG-400	LiTFSI: 36.5	PEG-400: 59.7	3.8	1:1.67	0.8 (25 ℃)	[9]

$LiMn_2O_4/Li_4Ti_5O_{12}$	2.37	Water/Acetonitrile hybrid electrolyte 15.3m LiTFSI in H_2O/AN (H_2O/AN =1:1, mass ratio)	LiTFSI: 81.4	AN: 12.9	5.7	1:1.15	2.99 (25 ℃)	[10]
$LiMn_2O_4/Li_4Ti_5O_{12}$	2.45	"Ether-in-Water" electrolyte 15m LiTFSI in H_2O/TEGDME (H_2O: TEGDME = 1:1.5, mass ratio)	LiTFSI: 82.2	TEGDME: 10.7	7.1	1:1.37	0.63 (25 ℃)	[11]
$LiMn_2O_4/Li_4Ti_5O_{12}$	2.45	"Hydrogen bond-anchored" electrolyte LiTFSI in sulfolane/H_2O (sulfolane: H_2O = 8:8, molar ratio)	LiTFSI: 50.8	Sulfolane: 42.7	6.5	1:2	2.5 (25 ℃)	[12]
$LiMn_2O_4/Li_4Ti_5O_{12}$	2.40	4.5m LiTFSI–KOH–$CO(NH_2)_2$–H_2O aqueous electrolyte (Urea: H_2O= 8.6:1, molar ratio)	LiTFSI: 56.4	Urea: 42.2	1.4	1:0.4	1.0 (25 ℃)	[13]
$LiMn_2O_4/NbO_2$	2.35	LiTFSI-H_2O-$MU_{0.27}$ (LiTFSI: H_2O: M-urea = 70: 54: 46)	LiTFSI: 82.1	Methylurea: 13.9	4.0	1:0.78	3.2 (25 ℃)	[14]
$LiMn_2O_4/Li_4Ti_5O_{12}$	2.45	9.5m LiTFSI-TMP-H_2O hybrid electrolytes	LiTFSI: 73.2	TMP: 21.9	4.9	1:1.07	1.0 (30 ℃)	[15]
$LiMn_2O_4/Zn_2Nb_{34}O_{87}$	2.43	50m LiTFSI + 30m TMBTFSI	LiTFSI: 52.7	TMBTFSI: 43.6	3.7	1:1.11	1.1 (30 ℃)	[16]
NCM811/ $Li_4Ti_5O_{12}$	2.2	40m LiTFSI + 20m EMImTFSI	LiTFSI: 56.5	EMImTFSI: 38.5	4.9	1:1.39	1.2 (25 ℃)	[17]
$LiNi_{0.5}Mn_{1.5}O_4/Li_4Ti_5O_{12}$	3.0	"Hydrogen bong-breaker" electrolyte LiTFSI: TMS: H_2O= 1:0.5:1	LiTFSI: 78.6	Sulfolane: 16.5	4.9	1:1	0.41 (25 ℃)	[18]

Table S5 The pH values for bare and LiH_2PO_4 treated TiO_2 electrode.

	initial	After 10 cycles at 0.5C
TiO_2	3.89	10.09
TiO_2@5%LHPO	2.30	8.18

Table S6 The performance parameters of the Ah-level LMO//TiO_2@5%LHPO pouch cell.

Capacity (mAh)	Voltage (V)	Weight energy density (Wh/kg)	Volume energy density (Wh/L)	Energy efficiency	Capacity retention after 400 cycles
1029	2.1	50.7	166.3	~90%	73.8%

Reference

[1] L. Suo, O. Borodin, T. Gao, M. Olguin, J. Ho, X. Fan, C. Luo, C. Wang, K. Xu, *Science* **2015**, *350*, 938-943.

[2] A. Zhou, J. Zhang, M. Chen, J. Yue, T. Lv, B. Liu, X. Zhu, K. Qin, G. Feng, L. Suo, *Adv. Mater.* **2022**, *34*, 2207040.

[3] L. Suo, O. Borodin, W. Sun, X. Fan, C. Yang, F. Wang, T. Gao, Z. Ma, M. Schroeder, A. von Cresce, S. M. Russell, M. Armand, A. Angell, K. Xu, C. Wang, *Angew. Chem. Int. Ed.* **2016**, *55*, 7136-7141.

[4] X. Hou, R. Wang, X. He, T. P. Pollard, X. Ju, L. Du, E. Paillard, H. Frielinghaus, L. C. Barnsley, O. Borodin, *Angew. Chem. Int. Ed.* **2021**, *60*, 22812-22817.

[5] Y. Yamada, K. Usui, K. Sodeyama, S. Ko, Y. Tateyama, A. Yamada, *Nat. Energy* **2016**, *1*, 1-9.

[6] S. Ko, Y. Yamada, K. Miyazaki, T. Shimada, E. Watanabe, Y. Tateyama, T. Kamiya, T. Honda, J. Akikusa, A. Yamada, *Electrochem. Commun.* **2019**, *104*, 106488.

[7] L. Chen, J. Zhang, Q. Li, J. Vatamanu, X. Ji, T. P. Pollard, C. Cui, S. Hou, J. Chen, C. Yang, L. Ma, M. S. Ding, M. Garaga, S. Greenbaum, H.-S. Lee, O. Borodin, K. Xu, C. Wang, *ACS Energy Lett.* **2020**, *5*, 968-974.

[8] F. Wang, O. Borodin, M. S. Ding, M. Gobet, J. Vatamanu, X. Fan, T. Gao, N. Eidson, Y. Liang, W. Sun, S. Greenbaum, K. Xu, C. Wang, *Joule* **2018**, *2*, 927-937.

[9] J. Xie, Z. Liang, Y. C. Lu, *Nat. Mater.* **2020**, *19*, 1006-1011.

[10] J. Chen, J. Vatamanu, L. Xing, O. Borodin, H. Chen, X. Guan, X. Liu, K. Xu, W. Li, *Adv. Energy Mater.* **2019**, *10*, 1902654.

[11] Y. Shang, N. Chen, Y. Li, S. Chen, J. Lai, Y. Huang, W. Qu, F. Wu, R. Chen, *Adv. Mater.* **2020**, *32*, e2004017.

[12] Y. Wang, T. Wang, D. Dong, J. Xie, Y. Guan, Y. Huang, J. Fan, Y.-C. Lu, *Matter* **2022**, *5*, 162-179.

[13] J. Xu, X. Ji, J. Zhang, C. Yang, P. Wang, S. Liu, K. Ludwig, F. Chen, P. Kofinas, C. Wang, *Nat. Energy* **2022**, *7*, 186-193.

[14] R. Lin, C. Ke, J. Chen, S. Liu, J. Wang, *Joule* **2022**, *6*, 399-417.

[15] Q. Li, C. Yang, J. Zhang, X. Ji, J. Xu, X. He, L. Chen, S. Hou, J. Uddin, D. Addison, *Angew. Chem. Int. Ed.* **2022**, *61*, e202214126.

[16] X. Zhu, M. Mao, Z. Lin, J. Yue, M. Li, T. Lv, A. Zhou, Y.-S. Hu, H. Li, X. Huang, *ACS Mater. Lett.* **2022**, *4*, 1574-1583.

[17] M. Becker, D. Rentsch, D. Reber, A. Aribia, C. Battaglia, R. S. Kühnel, *Angew. Chem. Int. Ed.* **2021**, *60*, 14100-14108.

[18] Y. Shang, S. Chen, N. Chen, Y. Li, J. Lai, Y. Ma, J. Chen, F. Wu, R. Chen, *Energy Environ. Sci.* **2022**, *15*, 2653-2663.